LITHOS 518–519 (2025) 108281

Contents lists available at ScienceDirect

LITHOS

journal homepage: www.elsevier.com/locate/lithos

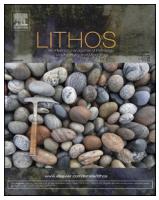

Subduction polarity reversals around the Solomon Island Arc associated with interaction of mantle domains in the Southwest Pacific

Rashmi Battan [a,b,c], Sun-Lin Chung [b,c,d,*], Tsuyoshi Komiya [e], Shigenori Maruyama [f], Truong Tai Nguyen [b,g], Hao-Yang Lee [b], Yoshiyuki Iizuka [b], Kwan-Nang Pang [b], Andrew Tien-Shun Lin [c]

[a] Taiwan International Graduate Program, Earth System Science, Academia Sinica, Taipei, Taiwan
[b] Institute of Earth Sciences, Academia Sinica, Taipei, Taiwan
[c] College of Earth Sciences, National Central University, Zhongli, Taoyuan, Taiwan
[d] Department of Geosciences, National Taiwan University, Taipei, Taiwan
[e] Department of Earth Sciences and Astronomy, University of Tokyo, Tokyo, Japan
[f] Department of Earth and Planetary Sciences, Tokyo Institute of Technology, Tokyo, Japan
[g] Department of Geology, Hanoi University of Mining and Geology, Hanoi, Viet Nam

ARTICLE INFO

Keywords:
Solomon Island arc
Subduction polarity reversal
Upper mantle domains
Southwest Pacific
Tectonic evolution

ABSTRACT

Subduction polarity reversal (SPR) leaves unique geochemical imprints in arc magmatic records, which serve as robust archives of magma-source evolution and the tectonic processes that shape magma genesis. This study reports zircon U—Pb ages, Hf isotopes, and whole-rock geochemical and Sr-Nd-Hf isotopic analyses of magmatic samples from the Solomon Island Arc (SIA) in the southwest Pacific, revealing three distinct stages of arc magmatism. Stage 1 (~46 Ma) comprises a set of low-K tholeiitic (TH) rocks from Santa Isabel and Choiseul. These rocks exhibit N-MORB-like geochemical signatures and display a Pacific mantle domain affinity in Hf—Nd isotopic space interpreted as arc magmatism involving partial melting of the mantle wedge above the NE-directed subduction of the Indo-Australian plate at the Pocklington Trough. Along with regional evidence, we suggest this as the first SPR in SIA, which may have begun as early as ~65 Ma, linked to changes in Pacific and Australian plate motion. Stage 2 (~35 Ma) is represented by low-K calc-alkaline (CA) granites from Ghizo, New Georgia Group (NGG), showing relatively unfractionated REE patterns, arc-like geochemical signatures, and Indian mantle-like isotopic affinity. This stage of magmatism reflects asthenospheric upwelling triggered by NE-directed slab break-off, followed by the arrival of the Louisiade Plateau at the Pocklington Trough and the onset of the second, SW-directed SPR. The slab break-off facilitated the generation of a juvenile arc pluton derived from an Indian-type upper mantle, which now constitutes the basement of NGG. Stage 3 (~19 Ma to 0.7 Ma) comprises a set of medium- to high-K CA rocks from NGG and Choiseul, with typical arc geochemical signatures (LILE and LREE enrichment and HFSEs depletion) and less positive εNd(t) (+5.8 to +7.2) and εHf(t) (+10.4 to +13.3) values than earlier stages. We infer a third SPR to have occurred ~19 Ma, following the ~20 Ma arrival of the Ontong Java Plateau (OJP) at the North Solomon trench (NST), thus initiating the interaction of OJP–Indian mantle domains. Together, these magmatic stages reveal recurrent SPR events and constrain the timing of the OJP–SIA collision that drove the latest SPR.

1. Introduction

SPR is one of the most commonly cited mechanisms for the subduction zone initiation (SZI), which itself remains one of the fundamental unresolved problems in modern plate tectonics theory (Cloetingh et al., 1989; Crameri et al., 2020; Stern, 2004; Stern and Gerya, 2018), with several competing mechanisms proposed. SPR involves the cessation of a previously active subduction zone due to the arrival of a buoyant block (oceanic plateau or continental fragment) at the trench, leading to the nucleation of a new subduction zone that dips in the opposite direction to the earlier subducting slab (Stern, 2004; Stern and Gerya, 2018). Cooper and Taylor (1985) first documented the presence

* Corresponding author at: Institute of Earth Sciences, Academia Sinica, Taipei, Taiwan.
E-mail address: sunlin@earth.sinica.edu.tw (S.-L. Chung).

https://doi.org/10.1016/j.lithos.2025.108281
Received 9 August 2025; Received in revised form 1 October 2025; Accepted 1 October 2025
Available online 12 October 2025

of two opposing dip directions beneath the Solomons. Other notable examples include the Luzon–Ryukyu SPR system near Taiwan (Chemenda et al., 2001; Clift et al., 2003; Teng et al., 2000) and the Vanuatu–Vitiaz SPR system in the New Hebrides region (Falvey, 1975). Yang (2022) introduced the term "subduction shield" that has encircled the Pacific Ocean since 180 Ma, preventing subduction-modified mantle from entering the region, except at the Chile Ridge in the Pacific Ocean. In contrast, SPR has also been proposed as a mechanism through which the mantle domain migration can take place from the Pacific to the African mantle domain (Doucet et al., 2020; Doucet and Li, 2024), a process often described as subduction infection or invasion (Mueller and Phillips, 1991; Duarte et al., 2013; Duarte et al., 2018). Similarly, Pearce et al. (2007) documented that the South Pacific Isotopic and Thermal Anomaly (SOPITA) mantle began influencing the southwest Pacific arc–back-arc system only after the OJP collision removed the subducting-slab barrier ~12 Ma.

SIA has been shaped primarily by the complex interactions between the Pacific and Indo-Australian plates (Schellart et al., 2006). The SPR (Cooper and Taylor, 1985) in the SIA and its collision with the oceanic plateau (Kroenke, 1984; Mann and Taira, 2004; Petterson et al., 1997) has gained considerable attention over the past decades (Shinohara et al., 2003; Schuth et al., 2011; Sun et al., 2021; Yang, 2022; Almeida et al., 2022 and Taylor and Benyshek, 2024). The SIA is considered an ideal natural laboratory for testing various paleo-reconstruction and numerical modeling to understand the tectonic evolution of SW Pacific better (Crawford et al., 2003; Schellart et al., 2006; Tapster et al., 2014; Matthews et al., 2015; Holm et al., 2016; Taylor and Benyshek, 2024; Van de Lagemaat and van Hinsbergen, 2024). Previous studies have proposed contrasting tectonic models and the timing of the SPR and OJP-SIA collision, summarized in Table S1. Two main models have been proposed: (i) Petterson et al. (1997, 1999) suggest 'soft docking' of the OJP with the NST at ~25–20 Ma, followed by a magmatic hiatus, SPR at ~8–7 Ma, and eventual 'hard docking' with major deformation between ~4–2 Ma in Malaita; (ii) Mann and Taira (2004), Phinney et al. (2004), and Cowley et al. (2004) propose a single tectonic event, with Pacific plate subduction continuing until ~5 Ma.

Intra-oceanic arc magmatism, through its geochemical signatures and precise chronology, can record mantle source shifts tied to polarity switches which can be useful to constrain the timing of OJP arrival at the NST and the subsequent SPR. An attempt has been made to evaluate how a changing tectonic regime beneath SIA affects magma-source composition (Schuth et al., 2009), but the scarcity of detailed geochronological, geochemical, and isotopic data from the SIA limits a comprehensive understanding of the spatio-temporal evolution of magmatism in this region, and the exact timing of the SPR, SIA-OJP collision. In this study, we re-evaluate existing tectonic models using new zircon U—Pb ages and Hf isotopic compositions, combined with whole-rock major and trace element and Sr-Nd-Hf isotopic data from the southern Santa Isabel, Choiseul, and the NGG within the SIA. By resolving the key issues, this study provides valuable insights into the spatio-temporal evolution of an island arc associated with SPR, the permeability of the Pacific "subduction shield", and the onset of externally sourced mantle inputs. Collectively, these advances refine the tectono-magmatic history of the southwest Pacific and provide a benchmark dataset for plate reconstructions, petrogenetic modeling, and comparative arc synthesis.

2. Geological background

The SIA trend northwest-southeast and forms a double chain of six major islands (Choiseul, Santa Isabel, Malaita, NGG, Guadalcanal and San Cristobal), spanning ~5°–12°S and 157°–163°E (Fig. 1). SIA is bounded to the north by the OJP and the Pacific Plate along the relict NST, a remnant of the former Vitiaz trench system and to the south by the Woodlark basin and the Indo-Australian Plate along the currently active SCT (Petterson et al., 1999). Owing to the geologically complex assemblage of crustal units (Petterson et al., 1997) and the lack of

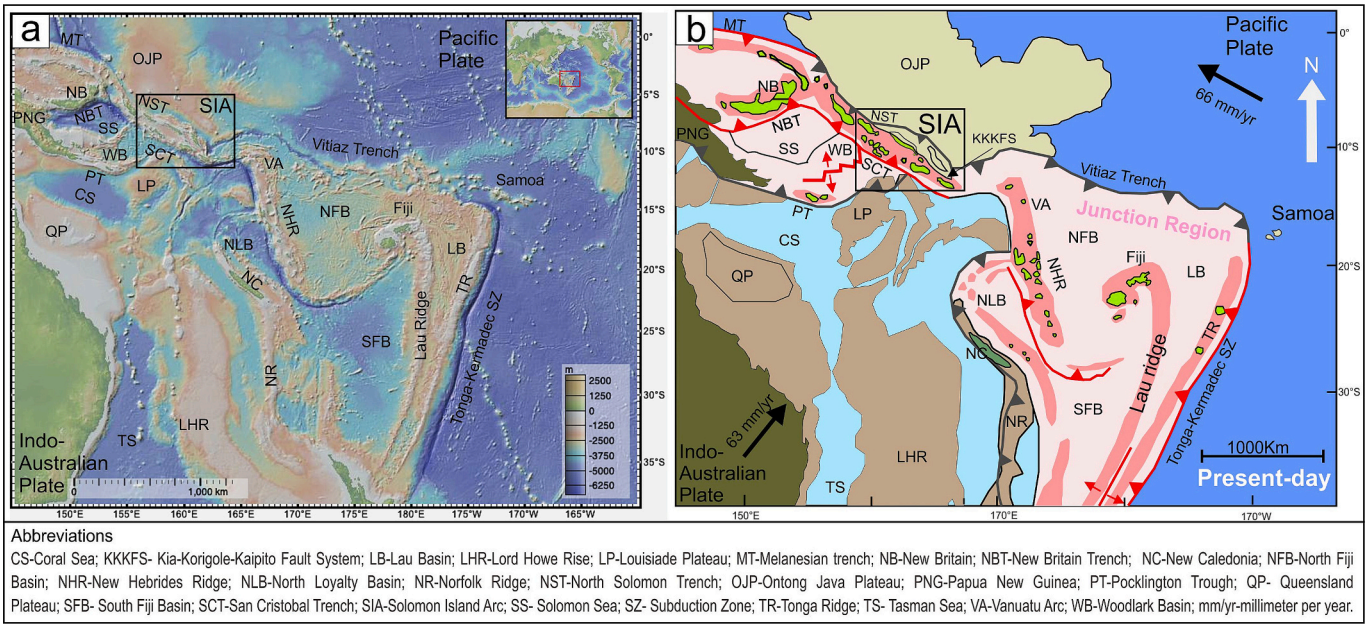

Fig. 1. (a) Ocean Bathymetry and topography map of the SW Pacific, modified from www.geomapapp.org. The bathymetric map highlights the complex mosaic of ridges, basins, and plateaus that control present-day plate interactions. The inset shows the regional context within the western Pacific. The black square marks the location of SIA. (b) Present-day tectonic configuration of the SW Pacific junction region, modified after Van De Lagemaat and Van Hinsbergen (2024), showing SIA situated between the Pacific and Indo-Australian plates. Red triangles mark active subduction zones, and thick black lines indicate inactive subduction zones. Plate convergence vectors indicate that the Pacific Plate is subducting westward beneath the Indo-Australian Plate at ~66 mm/yr in the north and 63 mm/yr in the south. Light pink shaded area highlights the broader junction region showing the extent of the Melanesian (SIA-Vanuatu-Fiji-Tonga–Kermadec) arc. Light green polygons indicate emergent island groups. The light brown color illustrates the extent of continental material rifted away from the Australian continent (in olive green) after the opening of the Tasman and Coral Sea (in light blue). The black arrows indicate the Pacific and Indo-Australian plate motion. Note: For higherresolution figure, readers are referred to web version of this article.

preserved forearc subduction channels, most estimates for the timing of SPR are derived from magmatic records, the opening of back-arc basins, and reconstructions of plate motion (Taylor and Benyshek, 2024). The temporal and spatial record of arc magmatism is highly heterogeneous, with notably distinct histories preserved in the SIA as discussed below for Santa Isabel, Choiseul and NGG.

2.1. Santa Isabel

The geology of Santa Isabel is illustrated in Fig. 2a. The island of Santa Isabel exposes a **juxtaposition of OJP and N-MORB-like terrain** (Petterson et al., **1999**). The basement of northern Santa Isabel is underlain by Sigana basalts dated ~90 Ma, which are chemically and isotopically identical to the OJP (Tejada et al., 1996). However, the San Jorge volcanics of the Jajao Igneous Suite in southern Santa Isabel, dated between ~62 and 46 Ma, exhibit N-MORB-like and arc–backarc geochemical characteristics. Their isotopic compositions plot within, or close to, the Pacific MORB field and notably lack Indian-MORB-like affinities. Tejada et al. (1996) interpreted them primarily as fragments of Pacific abyssal seafloor (~62 Ma) that were later obducted during OJP emplacement. Tapster et al. (2014) suggested that this arc-backarc magmatism was associated with the subduction of the Indo-Australian plate. Soon after ~45 Ma, the SW-directed subduction initiated beneath the Indo-Australian margin and leading to arc growth from New Britain to the Tonga-Kermadec system (Hall, 2002).

2.2. Choiseul

Coleman (1962) identified the Choiseul Schist as the oldest rock on the island, occurring in two variants (i) finely foliated and (ii) more granulose and described as amphibolites. Dating using K—Ar method on hornblende and plagioclase separates from the Choiseul basal schist yielded a mean age of 44 ± 18 Ma, marking the metamorphism of the protolith to amphibolitic schist (Richards et al., 1966). Subsequent work by Ramsay (1972) showed that the Choiseul Schist does not represent a precursor metamorphic event, but rather a sheared, metamorphosed, and uplifted equivalent of at least part of Voza lavas. Later, based on geological, geochronological and isotopic evidence Petterson et al. (1999) suggested that Choiseul has a Cretaceous N-MORB basement over which lies the arc magmatism from (i) Eocene to Early Miocene and (ii) Late Miocene to the present day. Geochronological constraints for the Choiseul basement and its two arc-magmatic stages remain undocumented. Berly (2005) identified that the Voza lava, Choiseul Schist, and Oaka Meta-microgabbro (a gabbroic intrusion restricted to southeastern Choiseul, as shown in Fig. 2b) all constitute the same unit, with a Pacific-like N-MORB origin. These basement rocks are mostly tholeiitic with minor calc-alkaline content (Coleman and Packham, 1976). The metamorphosed basement is unconformably overlain by the Siruka ultramafic complex, which is subsequently overlain by a sedimentary succession ranging from the Lower Miocene to the Pleistocene, as well as Quaternary volcanic deposits (Coleman, 1962). The younger volcanic sequence comprises typical calc-alkaline arc rocks, including basalts, andesites, and rhyolites (Petterson et al., 1999), and is likely associated with magmatism following the SPR along the SCT.

2.3. NGG

Unlike the Choiseul and Santa Isabel, the basement of the NGG remains ambiguous. Much of the southern island chain is composed of volcanic rocks that have formed within the last 6 Ma (Coleman, 1962; Chivas and McDougall, 1978; Abraham et al., 1987) after the late Miocene polarity reversal of subduction of the woodlark spreading ridge along the SCT (Dunkley, 1986; Ridgway, 1987) (Fig. 1). The oldest known magmatic rocks in the region have been dated to 2.3 ± 1 Ma (Petterson et al., 1999). This tectonic setting resulted in highly variable magmatism, including island-arc picrites, high-Mg andesite and adakites (Schuth et al., 2004, 2009; König et al., 2007; Smith et al., 2009) (Fig. 2c). Seismic tomography indicates the presence of two opposing subducting slabs beneath eastern NGG, suggesting complex subduction geometry beneath this segment of the arc (Taylor and Benyshek, 2024).

3. Samples

This study is focused on various types of magmatic rocks of the southern Santa Isabel, Choiseul, and the NGG. The geological map of each Island and sample locations are presented in Fig. 2. A total of 49 volcanic and plutonic rocks were selected for this study, 9 from southern Santa Isabel, 25 from Choiseul (plus three sand samples), and 15 from the NGG (Fig. 2), and are summarized in Table S2. The comprehensive data set is provided in Tables S1-S6. Due to dense vegetation cover and intense tropical weathering, most of them were collected along or from river exposures. Zircon U—Pb dating was conducted on 23 selected samples (Table S3); however, only 9 of these yielded zircon grains suitable for zircon Hf isotopic analysis (Table S4), as the remainder either had grains too small for laser ablation or exhibited a high Yb/Hf ratio. All 49 samples were analyzed for major and trace elements (Table S5). Whole-rock Sr-Nd-Hf isotopic analyses were carried out on 21 samples, 12 from Choiseul, 3 from Santa Isabel, and 6 from the NGG (Table S6).

3.1. Petrography

Gabbros from the Santa Isabel (Fig. S1a), Voza lava and Oaka Meta-microgabbros of Choiseul were first compared by Berly (2005). The major mineral phases are plagioclase and clinopyroxene with traces of opaque minerals. The absence of K-bearing phases and the intergranular texture are consistent with a tholeiitic basaltic composition. Whereas, the Choiseul amphibolites represent parallel and alternative bands of Plagioclase and hydrous minerals like amphiboles, with traces of opaque minerals. The basaltic andesites from Choiseul display randomly oriented plagioclase laths, interstitial pyroxene and hornblende and biotite. The Ghizo granites are composed of quartz, plagioclase, and variable amounts of hornblende. A diorite from Ghizo, display medium- to coarse-grained texture and contains plagioclase, hornblende, biotite, quartz, K-feldspar, and Fe—Ti oxides whereas an andesite from Ghizo, displays a porphyritic texture, with abundant plagioclase phenocrysts embedded in a groundmass of clinopyroxene. Vangunu monzodiorite contains plagioclase, quartz, and clinopyroxene, with notable quartz xenocrysts, suggesting it occupies a transitional composition between diorite and quartz monzonite. The petrography of representative samples is shown in Fig. S1.

4. Results

4.1. Geochronology

Zircon U—Pb isotopic analyses were performed with a Photon Machine Analyte G2 193 nm laser ablation system coupled with Agilent 7900 quadrupole ICP-MS, using a 30 μm laser spot size. Descriptions of the analytical methods used are given in Appendix A (Methodology). The zircon U—Pb isotopic data of the sample are listed in Table S3. The $^{207}Pb/^{235}U$ vs $^{206}Pb/^{238}U$ concordia diagrams for the analyzed samples are plotted in Fig. 3.

4.1.1. Santa Isabel

Zircons separated from a gabbro (SI78F) from southern Santa Isabel exhibit anhedral morphologies varying from prismatic to oval shapes, and CL images show weak oscillatory zoning and patchy textures. Most zircons range from 30 to 50 μm in size, with only a few reaching 70–100 μm, and their thin rims are generally unsuitable for crystallization age analysis. Their U and Th concentrations are listed in Table S3. Their Th/U ratio = 1, suggesting a magmatic origin, and yielded a concordant

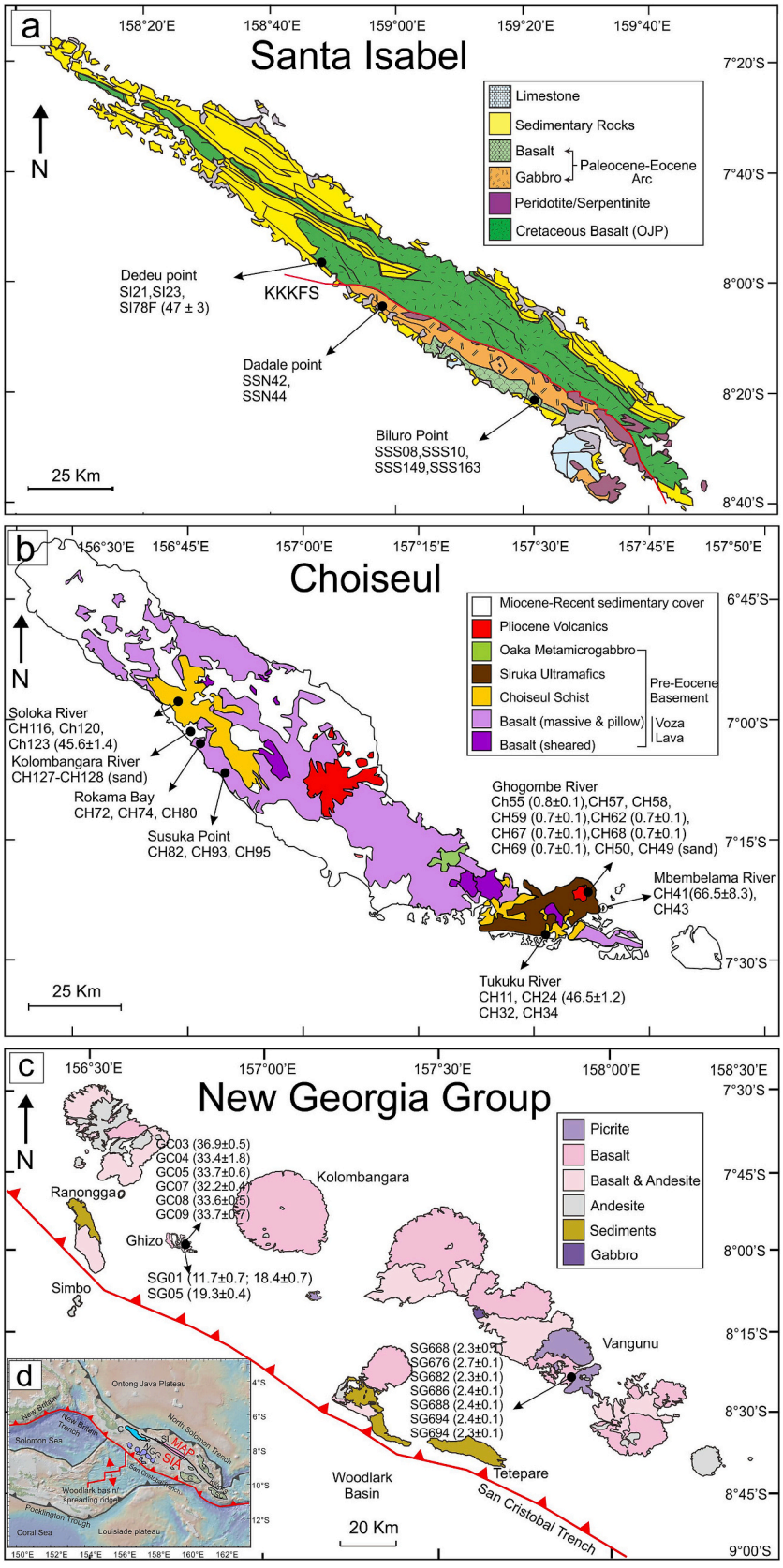

Fig. 2. Geologic map of (a) Santa Isabel (modified after Ota and Kaneko (2010). (b) Choiseul modified after Tapster et al. (2014), and (c) New Georgia Group (NGG) modified after Abraham et al. (1987). Black circles indicate sample collection sites, and ages shown are zircon U—Pb dates obtained from this study. Note: Please refer to the online version of this article for higherresolution figure.

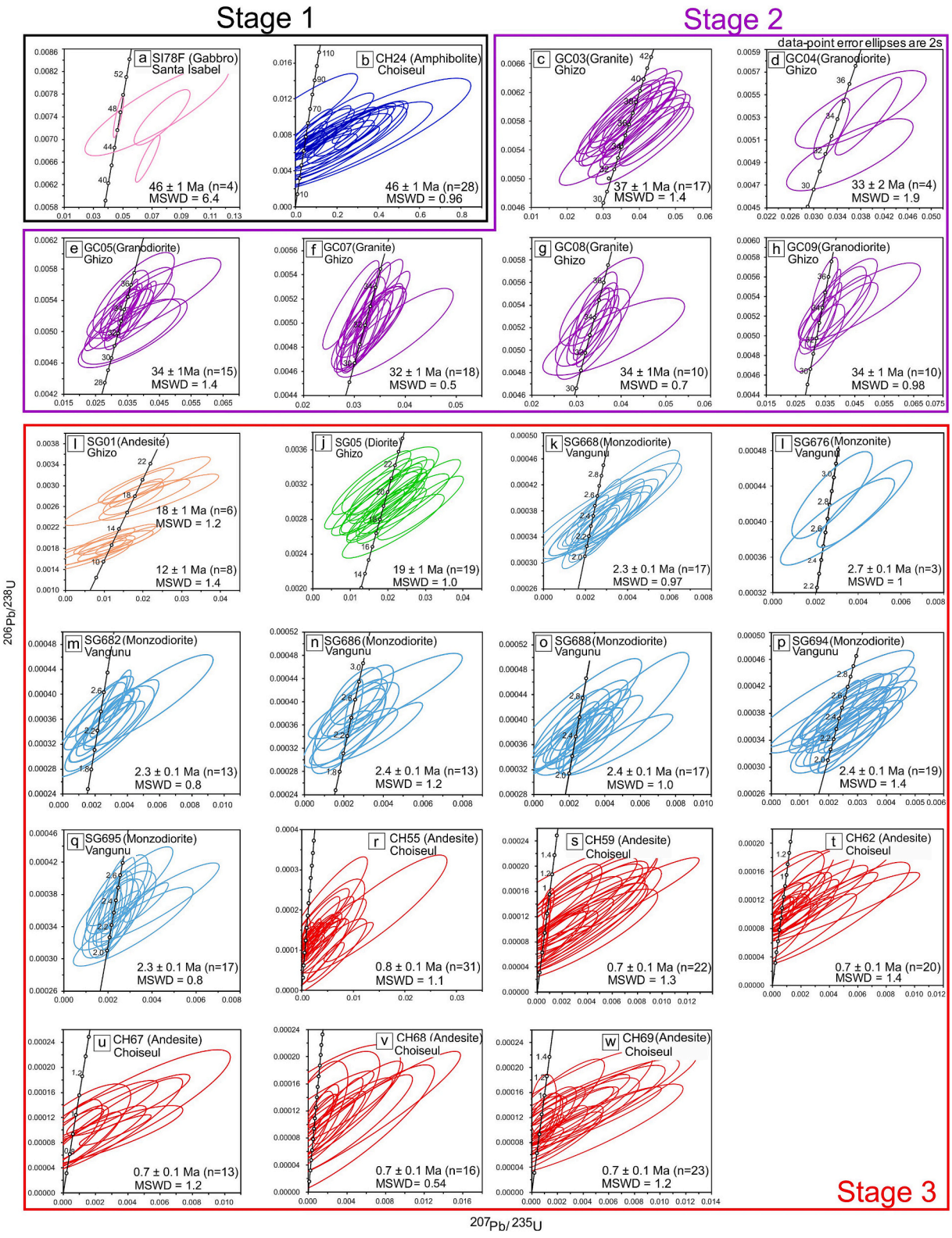

Fig. 3. Concordia plots of $^{207}Pb/^{235}U$ vs $^{206}Pb/^{238}U$ zircon age for Stage 1 (a, b) ~46 Ma magmatism in Santa Isabel and Choiseul, dated from a gabbro (SI78F) and an amphibolite (CH24), respectively. Stage 2 (c-h) ~35 Ma Ghizo granites mark another magmatic episode in SIA. Stage 3 (19 to <1 Ma) contains (i) Ghizo 19 Ma diorite (j) Ghizo 18,12 Ma andesite, Quaternary (k-q) ~2 Ma Vangunu monzodiorite and (r-w) ~0.7 (<1 Ma) Choiseul andesite. All uncertainties are presented with 2-sigma error at a 95 % confidence level. MSWD- mean squared weighted deviation. Note: Please refer to the online version of this article for higher resolution figure.

weighted mean $^{206}Pb/^{238}U$ age of 46.4 ± 1.2 Ma (n = 4) (Fig. 3a). Almost 20 out of 50 zircons yielded Neoproterozoic to Neoarchean inherited zircons. Thus, the Eocene ages obtained are considered to represent the timing of gabbro crystallization.

4.1.2. Choiseul

Zircons separated from an amphibolite (CH24) from Choiseul yielded a concordant weighted mean $^{206}Pb/^{238}U$ age of 46.5 ± 1.2 Ma (n = 28) (Fig. 3b). The zircons exhibit subhedral morphologies, typically prismatic to oval in shape. The grains are relatively small, varying between 30 and 50 μm in length, with none exceeding 100 μm. Their U and Th concentrations range from 2 to 17 ppm and 0.13–6.96 ppm, respectively. The Th/U ratios are mostly >0.3 except for a few grains showing values between 0.02 and 0.08. Detrital zircon grains from three sand samples collected along the rivers and beaches of Choiseul yielded two dominant age peak populations at 46.8 ± 0 0.4 Ma (n = 101) and 0.7 ± 0.1 Ma (n = 35) along with additional zircon ages ranging from the Late Eocene to Middle Miocene (Fig. S2). On the other hand, six basaltic andesites-andesite samples (CH55, CH59, CH62, CH67, CH68, CH69) from Choiseul yielded mean $^{206}Pb/^{238}U$ ages of 0.79 ± 1.05 Ma (MSWD = 1.1, n = 31), 0.74 ± 0.08 Ma (MSWD = 1.3, n = 22), 0.71 ± 1.04 Ma (MSWD = 1.4, n = 20), 0.71 ± 0.09 Ma (MSWD = 1.2, n = 13), 0.72 ± 0.06 Ma (MSWD = 0.5, n = 16), 0.73 ± 0.05 Ma (MSWD = 1.2, n = 23) all less than 1 Ma (Fig. 3r-w). Their Th/U ratios are >0.1, supporting a magmatic origin for the zircons.

4.1.3. NGG

Zircon separates obtained from six granites (GC03, GC04, GC05, GC07, GC08, GC09) of Ghizo Island, NGG yielded concordant weighted mean $^{206}Pb/^{238}U$ ages of 36.6 ± 0.5 Ma (MSWD = 0.88, n = 17), 33.4 ± 1.8 Ma (MSWD = 1.9, n = 4), 33.9 ± 0.6 Ma (MSWD = 1.8, n = 18), 32.2 ± 0.4 Ma (MSWD = 0.5, n = 18), 33.6 ± 0.5 Ma (MSWD = 0.7, n = 10), and 33.5 ± 0.5 Ma (MSWD = 1.09, n = 11) (Fig. 3c-h). The zircon grain size ranges from 50 to 150 μm, and their Th/U ratios are >0.1, suggesting a magmatic origin for these rocks. Their U and Th concentration are listed in the Table S3. Zircon grains from an andesite sample (SG01) from the same locality yielded two distinct concordant zircon age populations: 18.4 ± 0.7 Ma (MSWD = 1.2, n = 8) and 11.7 ± 0.5 Ma (MSWD = 1.4, n = 8) (Fig. 3i). A diorite (SG05) from Ghizo yielded a concordant $^{206}Pb/^{238}U$ weighted mean age of 19.3 ± 0.4 Ma (MSWD = 1.03, n = 19) (Fig. 3j). The presence of multiple age populations in SG01 suggests either prolonged magmatic activity or incorporation of antecrystic zircons from earlier intrusive phases. Seven Monzodiorite from Vangunu, NGG (SG668, SG676, SG682, SG686, SG688, SG694, SG695) yielded concordant mean $^{206}Pb/^{238}U$ ages of 2.3 ± 0.1 Ma (MSWD = 0.9, n = 17), 2.7 ± 0.1 Ma (MSWD = 1.0, n = 3), 2.3 ± 0.1 Ma (MSWD = 0.8, n = 13), 2.4 ± 0.1 Ma (MSWD = 1.2, n = 13), 2.4 ± 0.1 Ma (MSWD = 1.0, n = 17), 2.4 ± 0.1 Ma (MSWD = 1.4, n = 19), 2.3 ± 0.1 Ma (MSWD = 0.8, n = 17) (Fig. 6k-q).

4.2. Zircon Hf isotopes

4.2.1. Santa Isabel

In situ hafnium isotopic analysis of zircon grains dated from Santa Isabel was not feasible, as the grain sizes were smaller than the laser spot diameter. Consequently, Hf isotopic data could not be obtained for the dated zircons from Santa Isabel.

4.2.2. Choiseul

In situ hafnium isotopic compositions for zircon grains from the Choiseul are summarized in Table S4. The detailed descriptions of the analytical methods are presented in Appendix A. In situ hafnium isotopic analysis of ~46 Ma zircon grains dated from Choiseul was not feasible, as the grain sizes were smaller than the laser spot diameter. Consequently, Hf isotopic data could not be obtained for the dated zircons from Choiseul. Instead, detrital zircon grains from three sand samples were analyzed (Fig. S3) and plotted (Fig. 7a). The εHf(t) values for zircons younger than 1 Ma range from +12.6 to +10.1; those corresponding to the ~46 Ma population range from +15.1 to +9.6, and Middle Miocene zircon exhibit εHf(t) values between +13.1 and + 11.8. Zircons from six basaltic andesite samples (CH55, CH59, CH62, CH67, CH68, CH69) of Choiseul's youngest magmatism display a wide range for the εHf(t) values, ranging between +15.2 and + 9.7.

4.2.3. NGG

The in situ hafnium isotopic data of ~35 Ma Ghizo granite (GC03), yielded εHf(t = 35 Ma) values ranging between +16.9 to +13.2, plotted in Fig. 7a. Zircons from an andesite sample (SG01) display εHf(t) values between +13.1 to +11.1 and diorite (SG05), between +13.4 to +11.4. The seven Monzodiorite from Vangunu, NGG (SG668, SG676, SG682, SG686, SG688, SG694, SG695) couldn't be analyzed due to a high Yb/Hf ratio. In situ hafnium isotopic compositions for zircon grains from the NGG are summarized in Table S4.

4.3. Whole-rock major and trace elements

Whole-rock trace elements data from Santa Isabel, Choiseul, and NGG are presented in Table S5.

Detailed descriptions of the geochemical methods used in this study are presented in Appendix A. Forty-nine representative samples were selected for whole-rock major element analysis, summarized in Table S5. Samples from Santa Isabel exhibit relatively high loss on ignition (LOI) values, ranging from 0.32 to 4.31 wt%, while those from Choiseul show lower LOI values (0.41 to 2.74 wt%), except for sample CH58, which shows an anomalously high LOI of 6.85 wt%, likely reflecting secondary alteration or elevated volatile content. Samples from NGG display LOI values (0.2 to 2.98 wt%), indicating variable degrees of post-magmatic alteration and/or hydration. The ~46 Ma samples of Santa Isabel and Choiseul show basic affinities on the TAS diagram (Fig. 4a) with SiO_2 (49.05 to 51.52) wt% and total alkalis ranging from 2.89 to 5.07 wt% for Santa Isabel and between 47.14 and 53.71 wt% and 2.46 to 6.44 wt% for Choiseul. These samples fall in the low-K TH field on silica content versus K_2O wt% diagram as illustrated in Fig. 4b, with K_2O contents ranging between 0.05 and 0.37 wt% in Santa Isabel, and (0.08–1.60) wt% in Choiseul. Whereas, the basaltic andesite-andesite samples from Choiseul have intermediate silica and total alkalis content (55.66–58.48) and (5.85–6.18) (Fig. 4a) and plot in high-K CA series (Fig. 4b) with K_2O (2.20–2.25) wt%. The ~35 NGG samples are most evolved with the highest silica content between 71.83 and 76.24 wt% and total alkalis (3.85–6.36) wt% with K_2O (0.07–0.45) wt%, showing low-K TH affinities, whereas the diorite, andesite and monzodiorite samples display intermediate silica content with 53.70 to 62.27 wt% with total alkalis ranging between 5.28 and 6.74 wt%, and has medium to high K_2O (1.31 to 2.25) wt% akin to Choiseul basaltic-andesite to andesites (Fig. 4a and b).

Chondrite-normalized rare earth element (REE) patterns and trace elements normalized to normal mid-ocean ridge basalt (N-MORB) are according to Sun and McDonough (1989) (Fig. 5). The ~46 Ma, samples from Santa Isabel and Choiseul exhibit light REE depletion relative to heavy REE, accompanied by a negative europium (Eu) anomaly in Santa Isabel and slightly negative for Choiseul samples. In N-MORB-normalized trace element diagrams, these samples display variable enrichment in large ion lithophile elements (LILEs; e.g., Rb, Ba) and slight depletion in high field strength elements (HFSEs), particularly Niobium (Nb) and Tantalum (Ta) (Fig. 5a and b and Fig. S2). However, the <1 Ma samples from Choiseul show enrichment of light REEs over heavy REEs, no significant Eu anomaly, enrichment in LILEs, and pronounced depletions in HFSEs (e.g., Nb, Ta, and Ti) in N-MORB-normalized multi-element diagrams (Fig. 5f). The ~35 Ma, NGG samples show a flat REEs pattern with more pronounced negative Eu anomaly, except one sample, GC08, showing a positive Eu anomaly. All samples exhibit substantial enrichment in LILEs (e.g., Rb, Ba) and notable depletion in Pb. HFSEs (e.g., Nb,

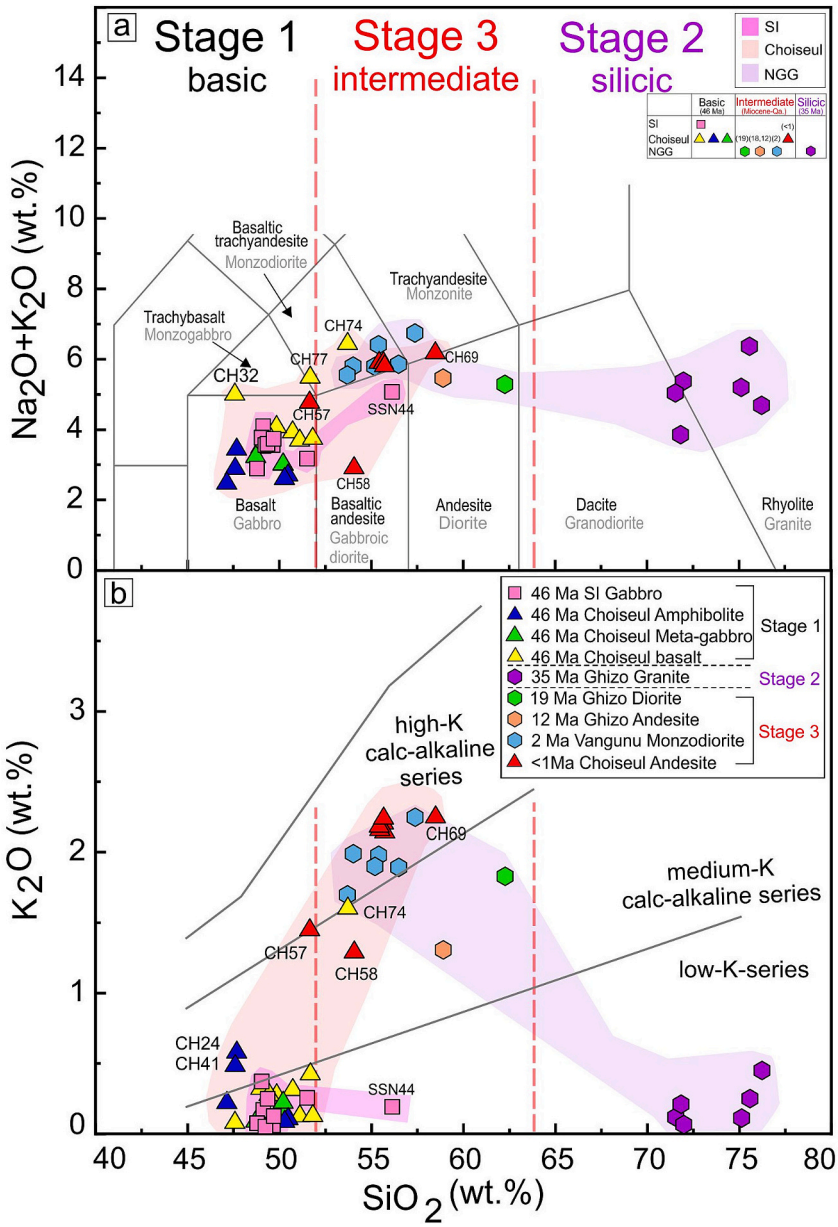

Fig. 4. (a) Total alkali (Na_2O + K_2O) versus SiO_2 (TAS) diagram classified according to Le Maitre et al. (2005). (b) K_2O versus SiO_2 diagram after Peccerillo and Taylor (1976). The ~46 Ma Stage 1 is basic and falls in low-K TH, ~35 Ma Stage 2 is silicic and plots in the low-K-CA. Stage 3 (19 to <1 Ma) shows intermediate SiO_2 content and plots in the medium to high-K CA series.

Ta, Ti) are relatively depleted (Fig. 5c). On the contrary, the 19–2 Ma samples from NGG show enrichment of light REEs over heavy REEs with no significant Eu anomaly except SG05, showing a negative Eu anomaly and pronounced depletions in HFSEs (e.g., Nb, Ta, and Ti) in N-MORB-normalized multi-element diagrams (Fig. 5d-e).

4.4. *Whole-rock Sr-Nd-Hf isotopes*

Whole-rock Sr-Nd-Hf isotopic data are listed in Table S6. To minimize the effect of alteration, samples were first screened petrographically and those with the freshest mineralogy were prioritized for isotopic analysis. In geochemical interpretations, emphasis was placed on immobile trace elements (e.g., HFSEs, REEs), while mobile LILEs (Rb, Ba, Sr) were treated with caution. A total of 21 samples, 12 from Choiseul, 3 from SI, and 6 from NGG were selected for whole-rock Sr-Nd-Hf isotopic analyses. The variation of Sr-Nd-Hf isotopes with SiO_2 contents is illustrated in Fig. 6. The ~46 Ma samples from Santa Isabel and Choiseul exhibit a wide range of initial Sr isotopic ratios i.e. $(^{87}Sr/^{86}Sr)_i$ from 0.7030 to 0.7045 and from 0.7026 to 0.7048 (Fig. 6a), respectively, when plotted against silica content. These samples display the most depleted εNd(t) values from +8.5 to +8.8 and + 8.2 to +8.7 (Fig. 6b), while εHf(t) values range from +11.9 to +12.6 and + 10.4 to +14.4, respectively. The <1 Ma samples from Choiseul exhibit a narrower range of $(^{87}Sr/^{86}Sr)_i$ ratios from 0.7037 to 0.7043 and most evolved εNd(t) values ranging from +6.2 to +5.8 (Fig. 6b) and εHf(t) values between +11.3 to +10.4. The ~35 Ma granites from Ghizo show a narrower $(^{87}Sr/^{86}Sr)_i$ ratios ranging from 0.7035 to 0.7042, εNd(t) value of +7.7 and highly depleted εHf(t) values between +15.2 to +15.9 (Fig. 6c). In contrast, the 19–2 Ma samples show $(^{87}Sr/^{86}Sr)_i$ ratios ranging from 0.7035 to 0.7037, εNd(t) value of +6.8 to +5.8 and εHf(t) values between +13.5 to +11.5. The whole-rock εHf(t) values are plotted for comparison with zircon εHf(t) values from ~46 to <1 Ma samples from Santa Isabel, Choiseul, and NGG, along with detrital zircon εHf(t) values from Choiseul (Fig. 7a).

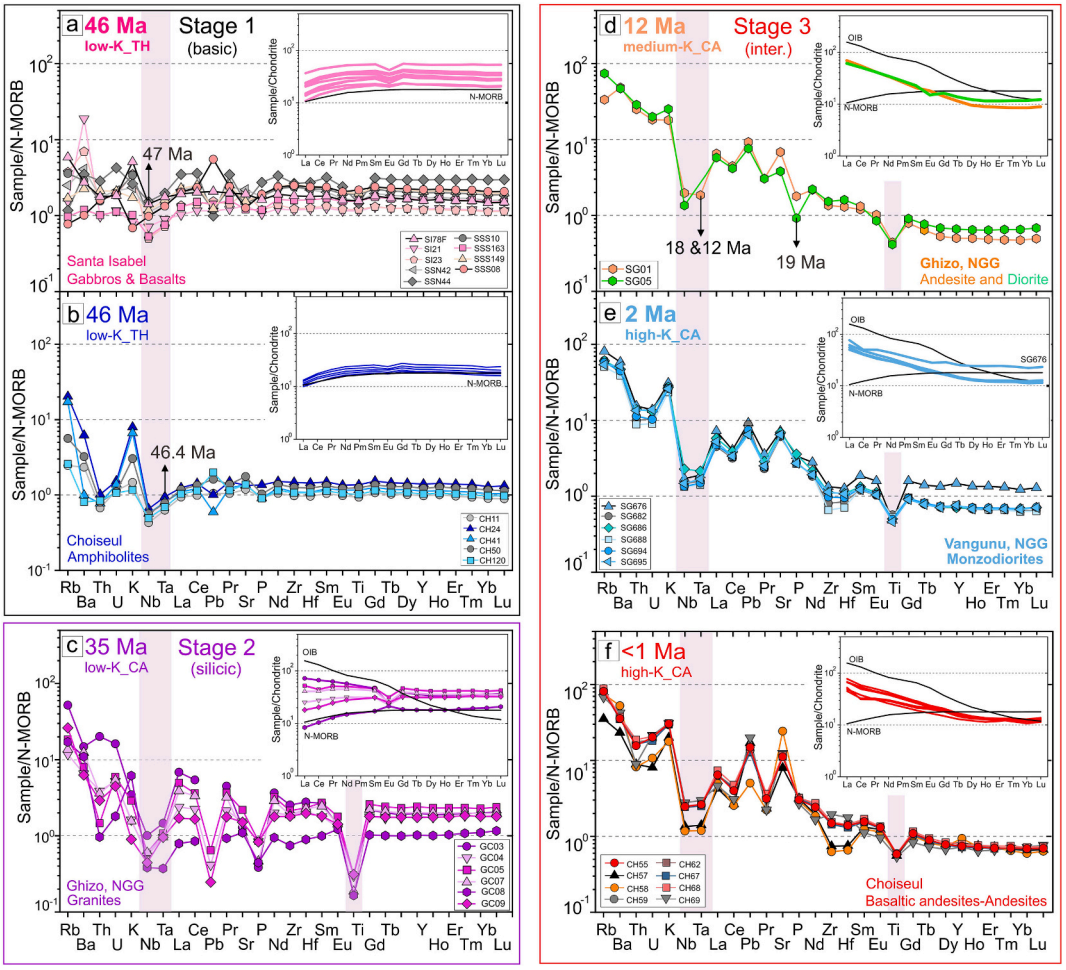

Fig. 5. N-MORB normalized spidergrams for (a) Santa Isabel, (b and f) Choiseul and (c-e) NGG with chondrite-normalized rare earth element (REE) patterns as insets in top right corners (a-f). (a, b) ~46 Ma Stage 1 low-K TH arc magmatism in Santa Isabel and Choiseul, (c) ~35 Ma Stage 2 low-K CA Ghizo granites and (d-f) Stage 3 medium to high-K CA arc magmatism in Vangunu (NGG) and Choiseul. The chondrites and N-MORB normalization values are from Sun and McDonough (1989). Note: Please refer to the online version of this article for higher resolution figure.

5. Discussion

5.1. Crustal contamination and magma source

The ($^{87}Sr/^{86}Sr$)i, positive εNd(t) and εHf(t) values for Santa Isabel, Choiseul and NGG with varying SiO_2 contents (Fig. 6a-c) suggest derivation from a depleted mantle source and insignificant or negligible crustal contamination during magma evolution. A similar conclusion can be based on the zircon in situ positive εHf(t) values (Fig. 7a) for all the studied samples from SIA, which also indicate a lack of crustal contribution during magma ascent. We conclude that incompatible elemental and isotopic ratios were unaffected during magma ascent, and can therefore be used to determine the nature of the source region.

5.2. Petrogenesis

Our new zircon U—Pb ages, Hf isotopic compositions, integrated with whole-rock elemental and isotopic data, enabled us to classify the obtained ages as Stage 1, Stage 2 and Stage 3 of arc magmatism in SIA, inferred from Santa Isabel, Choiseul, and NGG. Stage 1 arc magmatism, dated at ~46 Ma, is characterized by basic, low-K TH) samples from Santa Isabel and Choiseul, indicating early arc magmatism. Stage 2 arc magmatism, dated at ~35 Ma, marked by highly silicic, low-K CA granites from Ghizo (NGG), reflecting a more evolved magmatic phase. Stage 3 arc magmatism spans from 19 Ma to <1 Ma and is represented by intermediate rocks showing medium to high-K CA affinity from both NGG and Choiseul. These stages are discussed in detail in the following sections.

5.2.1. Stage 1 arc magmatism

The ~46 Ma samples from Santa Isabel and Choiseul represent "Stage 1" arc magmatism in the SIA. These rocks are basic, low-K TH in composition (Fig. 4a and b) and display N-MORB-like REE patterns (depleted LREEs over HREEs), slight enrichment in LILEs, and depletion in HFSEs like Nb and Ta in trace element pattern (Fig. 5a and b). Both islands display depleted whole-rock Sr-Nd-Hf isotopic signatures that are nearly identical, suggesting their derivation from a juvenile Pacific MORB-like mantle source (Fig. 6) with no involvement of older continental crust, consistent with an intra-oceanic arc-backarc setting. The Stage 1 samples fall within the Pacific mantle domain in εNd(t) vs εHf(t) correlation diagram by Pearce et al. (2007), illustrated in Fig. 7b, suggesting that the upper mantle characteristics at ~46 Ma were Pacific MORB-like. The three amphibolite samples lie on the discrimination line, which might be an indicator of seawater alteration.

5.2.2. Stage 2 arc magmatism

The ~34 Ma granites from Ghizo (NGG) have I-type affinity and represent "Stage 2" arc magmatism in the SIA. Unlike the earlier Stage 1 magmatism, Stage 2 samples are more silicic and characterized by low-K CA composition (Fig. 4a and b). They display nearly flat REE patterns

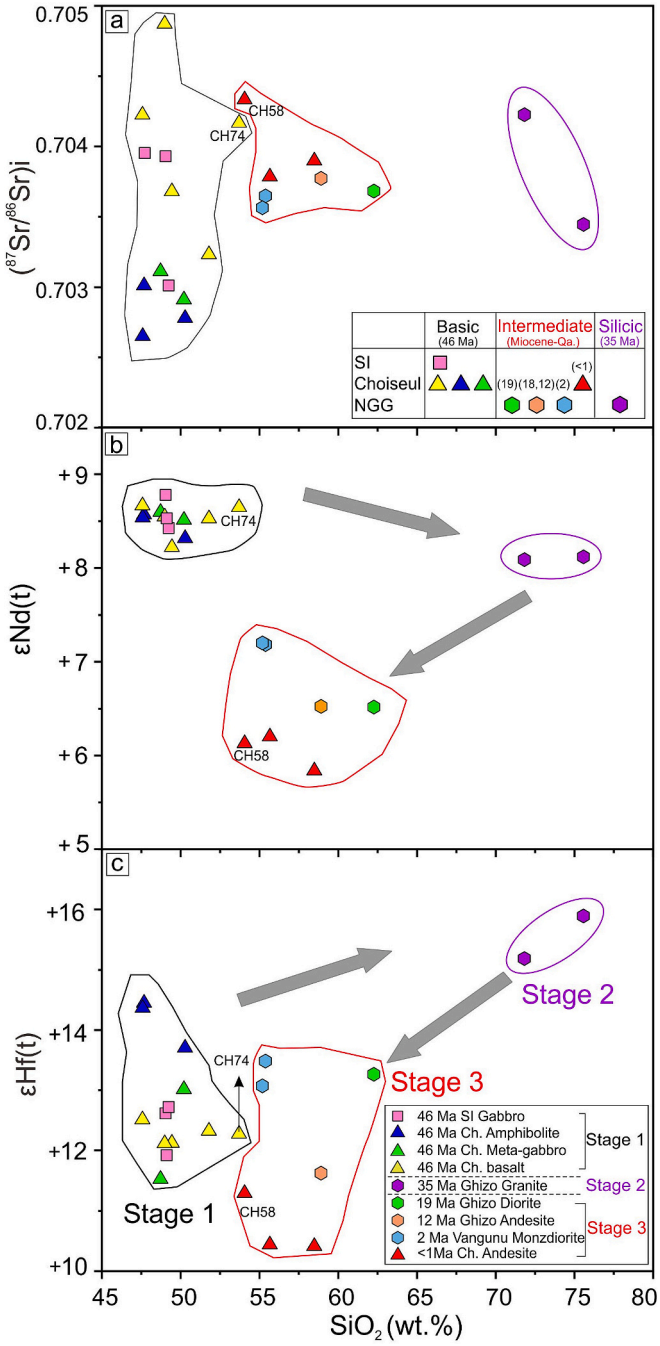

Fig. 6. SiO_2 (wt%) vs. (a) $^{87}Sr/^{86}Sr(i)$, (b) εNd(t) and (c) εHf(t) of magmatic rocks from SIA showing variation from Stage 1 to Stage 3. These variations illustrate the spatio-temporal evolution of magma source composition from ~46 Ma to <1 Ma, suggesting changes in the tectonic environment associated with subduction polarity reversals.

with prominent enrichment in LILEs and depletion in HFSEs (Fig. 5c), marking a clear elemental composition shift from Stage 1 to Stage 2. Corresponding shifts in whole-rock Sr-Nd-Hf isotopic ratios (Fig. 6a-c) and zircon εHf(t) values (Fig. 7a) further highlight a change in magma source plausibly due to change in tectonic environment around ~35 Ma or before it. The initial εNd(t) and εHf(t) values suggest that the Ghizo granites were derived from an upper mantle source with isotopic characteristics similar to the Indian mantle domain. The whole-rock elemental (Fig. 5c) and isotopic composition (Figs. 6 and 7) together with zircon εHf(t) values (Fig. 7a) suggest a juvenile mantle source and effectively rule out any significant interaction with continental fragments during magma genesis in this stage.

5.2.3. *Stage 3 arc magmatism*

The ~19 to 2 Ma rocks from NGG and < 1 Ma samples from Choiseul mark the onset of "Stage 3" and a mature arc magmatism. These rocks are intermediate in silica content and belong to the medium to high-K CA series (Fig. 4a and b). They exhibit typical island arc-like REE patterns, with pronounced LREE enrichment relative to HREE, variable enrichment in LILEs, and pronounced subduction-related signatures such as depletion in HFSEs i.e. Nb, Ta and Ti (Figs. 5d-f). The Hf and Nd isotopic compositions of the Stage 3 samples from Choiseul and the NGG fall within the Indian mantle domain and closely overlap with the OJP basalts field, indicating their derivation from an Indian-type mantle source influenced by the OJP upper mantle domain (Fig. 7b).

5.3. *Tectonic evolution of the SIA*

Understanding the spatial and temporal evolution of the SIA requires insights into tectonic events predating the ~46 Ma Stage 1 arc-backarc magmatism. Numerous tectonic reconstruction models for the SW Pacific (Crawford et al., 2003; Schellart et al., 2006; Whattam et al., 2008; Holm et al., 2016; Matthews et al., 2015; Van de Lagemaat and van Hinsbergen, 2024) have addressed possible tectonic setting, timing for previous subduction initiation, and interaction between the Pacific and Australian plates. We attempt to assess the validity of earlier proposed timings for SPR and OJP-SIA collision based on our newly acquired U—Pb and geochemical-isotopic datasets.

5.3.1. *Pre-Arc Basement formation (before 85 Ma)*

Tectonic reconstruction models suggest that a southwest-directed subduction of the Pacific plate existed in the southwest Pacific before 85 Ma (Van de Lagemaat and van Hinsbergen, 2024). The ophiolitic crust from Guadalcanal is dated at 92 ± 20 Ma by the K/Ar method (Ridgway, 1987) and formed during the Cretaceous within a back-arc basin, driven by the rollback of the Pacific slab along the continental margin (Schellart et al., 2006). This interpretation is corroborated by ~96 Ma zircon population obtained from 26 to 24 Ma pluton on Guadalcanal (Tapster et al., 2014). A major change in plate motion occurred around 85 Ma, when the Pacific plate shifted ~700 km to the northwest. This movement led to the termination of south-directed subduction ~85 Ma, and initiated a transform plate boundary between the Pacific and Indo-Australian plates, marking a significant shift in regional tectonic configuration (Van de Lagemaat and van Hinsbergen, 2024). Subduction-related evidence in the Junction region (Fig. 1) is sparse from 85 to 62 Ma.

5.3.2. *First SPR (~62–46 Ma) associated with the Pacific-type mantle domain*

The onset of the first SPR is recorded in (~ 46 Ma) Stage 1 arc-backarc magmatism (Fig. 8a). These samples are derived from a juvenile mantle source (Fig. 6a-c) with εNd(t) and εHf(t) isotopic characteristics of a Pacific-type mantle domain (Fig. 7b). The tectonic setting corresponds to the initiation of a northeast-directed subduction of the Indo-Australian plate ~62 Ma, at known as the Pocklington trough (Tapster et al., 2014). The NW-directed subduction initiated due to a modest change in the absolute plate motion of the Pacific plate and major changes in Australian plate motion ~65 Ma (Kroenke et al., 2004). This timing is further supported by $^{40}Ar—^{39}Ar$ ages from the Santa Isabel ophiolitic assemblage yielding ~62 and 46 Ma, and displays Pacific MORB-like Sr-Nd-Pb isotopic and chemical affinities (Tejada et al., 1996). The magmatic hiatus from 62 to 50 Ma could have resulted from slow and limited relative motion between the Pacific and the Indo-Australian plates (Van de Lagemaat and van Hinsbergen, 2024). The initial Nd isotopic ratios range from +7.9 to +8.8 for Choiseul schist and Voza lava. The gabbro from San Jorge shows a value of +6.3 while the Oaka microgabbro from Choiseul has a value of +8.2 (Berly, 2005).

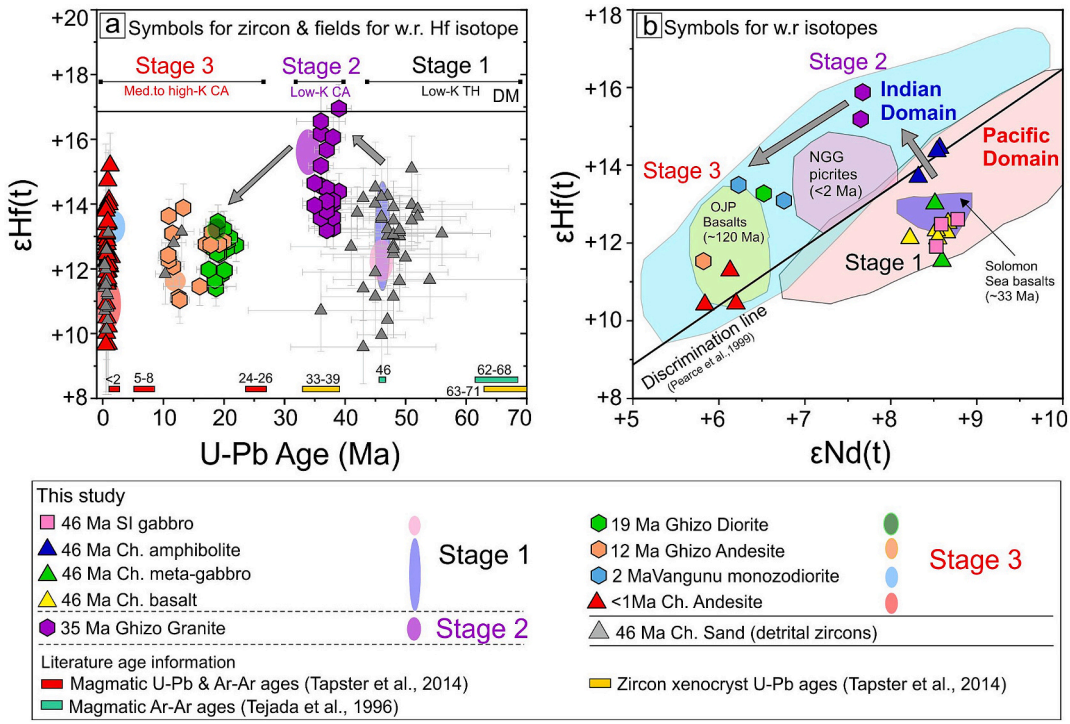

Fig. 7. (a) Zircon U—Pb ages vs zircon εHf(t) as solid symbols and whole-rock zircon εHf(t) as colored fields, triangles show detrital zircon εHf(t) values from Choiseul. The data from the SIA predominantly indicate a juvenile source for SI, Choiseul and NGG islands with significant changes in magma source composition from Stage 1–3. Stage 2 samples exhibit the highest radiogenic εHf(t) close to depleted mantle (DM). The depleted mantle array is after Chauvel and Blichert-Toft (2001). (b) whole-rock εHf(t) vs εHf(t) showing change of mantle domain from ~46 Ma stage 1 low-K tholeiitic samples from Santa Isabel and Choiseul to ~35 Ma low-K calc-alkaline silicic granites from Ghizo. Another change of mantle domain is marked by Stage 3 intermediate rocks with medium to high-K calc-alkaline content from the Indian-type to the OJP-type mantle domains. The Indian and Pacific mid-ocean ridge basalts data compiled from Stracke et al. (2022). Solomon Sea basalts are from Pearce et al. (2007) and εHf(t) versus εNd(t) discrimination line in from (Pearce et al., 1999).

Similarly, the Koloséru gabbros from Santa Isabel/San Jorge yielded εNd (t = 60 Ma) values of +7.8 (Tejada et al., 1996). Our results, integrated with existing literature data, suggest the possibility of synchronous Stage 1 arc magmatism on both Santa Isabel and Choiseul, indicating a regional magmatic response to the onset of the first SPR.

5.3.3. *Second SPR (~35 Ma) associated with the Indian-type juvenile crust*

The onset of the second SPR reversal is recorded in (~ 35 Ma) Stage 2 arc magmatism (Fig. 8b). These samples are derived from a juvenile mantle source (Fig. 6a-c) with isotopic characteristics of an Indian-type mantle domain (Fig. 7b) above a southwest-directed subduction of the Pacific plate at NST (Fig. 8b). The spatio-temporal elemental (Fig. 5a-c), isotopic shifts (Fig. 6a-c, 7a and 7b) is a clear indication of change in tectonic setting as well as magma source composition from Stage 1 to 2 arc magmatism. The northeast-directed subduction terminated after an Eocene interaction of a continental fragment (or possibly the Louisiade Plateau) with SIA (Tapster et al., 2014) and a southwest-directed subduction initiation or second SPR led to the formation of the ~35 Ma basement of NGG. Arc magmatism associated with this subduction is recorded between 38 and 35 Ma in Small Nggela, Florida groups (Neef and McDougall, 1976); and possibly in Guadalcanal as well, as evidenced by zircon xenocryst population of 39–33 Ma and 26–24 Ma plutons from Guadalcanal (Tapster et al., 2014). Additional evidence for southwest-directed subduction comes from the timing of Solomon Sea spreading ~33–28 Ma (Joshima et al., 1986) as a back-arc basin due to Pacific-slab rollback (Schellart et al., 2006; Tapster et al., 2014). After ~45–40 Ma, the NE-directed subducting slab at Pocklington trough broke off and a SW-directed subduction re-initiated. The NE-directed slab break-off likely facilitated the upwelling of hotter asthenospheric mantle, resulting in ~35 Ma emplacement of Stage 2 arc plutons in NGG with an Indian-like mantle domain and magmatic activity recorded in other islands of SIA as discussed above. The highly silicic nature and depleted isotopic signatures of these granites may indicate that mantle-derived mafic magmas were possibly subsequently modified through assimilation and fractional crystallization (AFC) within the crust, which could account for their genesis. At the same time, the isotopic contrast between an Indian-type mantle domain in Stage 2 magmatism from the NGG and a Pacific-type mantle domain of the Solomon Sea basalts (Fig. 7b) highlights a more complex mantle configuration beneath the SIA.

5.3.4. *Third SPR (~19 Ma) linked to Indian-type mantle and OJP-SIA collision*

Another shift in magma source characteristics is evident in Stage 2 magmatism. The 19 Ma Ghizo diorite, together with bimodal andesite ages of 18 and 12 Ma from Stage 3 magmatism, marks the onset of changes in geochemical and Indian-type isotopic composition and the initiation of typical subduction-related arc magmatism in the Ghizo and NGG. The southwest-directed subduction of the Pacific plate halted after the initial contact of OJP at NST ~20 Ma (Fig. 8c) (Petterson et al., 1997; Petterson et al., 1999; Hall, 2002; Schellart et al., 2006; Holm et al., 2013). However, in the SW Pacific, Melanesian arc volcanism related to Pacific Plate subduction at the Vitiaz Trench was terminated between 13.6 and 12.7 Ma in the western belt of Vanuatu (Taylor and Benyshek, 2024). This might suggest that the OJP arrival at Vitiaz or NST was not uniform along the trench margin; instead, its edges appear to have collided with the trench at different times and locations. The Pacific-like isotopic signature of Malekula segment of the Vanuatu arc till ~20 Ma (Haase et al., 2024a) also suggests the same. Before this study, there was no evidence that the modern polarity arc volcanism began no earlier than 8 Ma in the Solomon Islands (Petterson et al., 1999). However, our data suggest that the third or most recent SPR likely initiated ~19 Ma, as

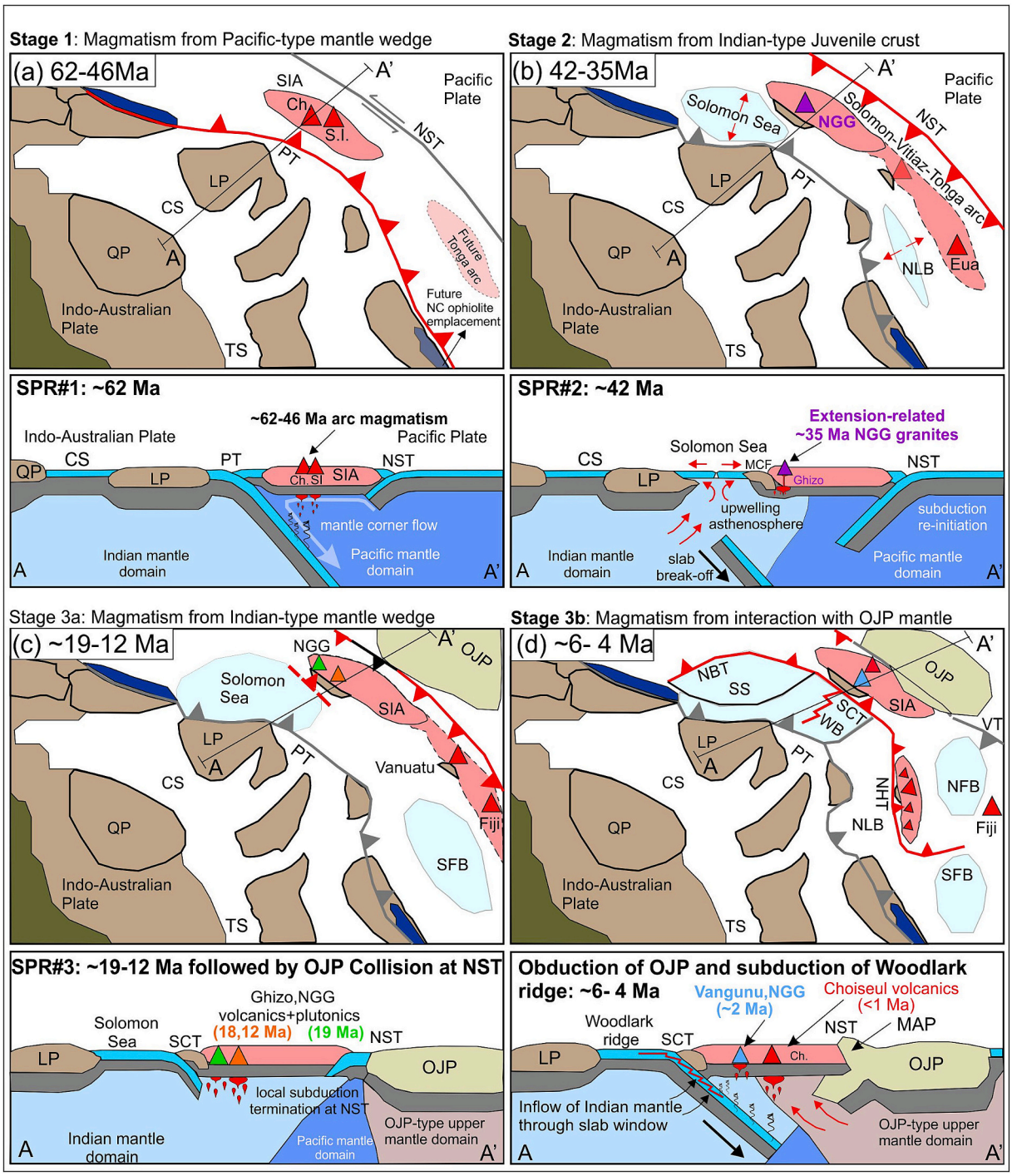

Fig. 8. Paleogeographic construction of SIA, SW Pacific from ~62 to present modified from Tapster et al. (2014). Cross-sections along profile A-A' are also shown below.

inferred from the Ghizo diorite. A systematic decline in εHf(t = 35 Ma) to εHf(t = 19 Ma) values from both zircon (Fig. 7a) and whole-rock isotopic data indicates a shift in mantle source characteristics (Figs. 6 and 7), reflecting a change in magma source after ~35 Ma to 19 Ma and remains the same until <1 Ma. The enrichment of LREE, LILEs and less depleted isotopic values of εNd(t) and εHf(t) suggest a third SPR. The Stage 3 magmatic samples plot close to and overlap with the OJP basalt field by Tejada et al. (2002), suggesting that the OJP-type mantle material started to spread beneath SIA more prominently after 19 Ma.

The ~2 Ma Vangunu monzodiorite and the <1 Ma Choiseul andesites of Stage 3 magmatism plot within the Indian-type mantle domain and close to the OJP-basalt field (Fig. 7b). We interpret that the arc magmatism was formed from an Indian-mantle wedge overprinted by an OJP-type upper mantle domain. The "hard docking" of OJP at the NST ~4 Ma (Petterson et al., 1997, 1999) and extensive deformation of the OJP basement and formation of the Malaita anticlinorium (Kroenke, 1972) or MAP ~4 Ma (Phinney et al., 2004) resulted in the inflow of the OJP material i.e. OJP-type upper mantle domain beneath SIA. This Indian-type mantle domain continued through a slab window within the subducting Woodlark Ridge, resulting in hybrid mantle sources that contributed to the observed geochemical diversity in late-stage arc magmatism. We suggest the possibility of initiation of latest SPR in SIA

initiated between no earlier than 19 Ma and no later than 12 Ma (Fig. 8). This finding is also supported by supported by $^{40}Ar/^{39}Ar$ ages of hornblende andesite dated at ~7.7–5.2 Ma from Gallego Volcanic field and the Gold ridge volcanic, Guadalcanal (Tapster, 2013), marking the oldest arc magmatism from the latest SPR.

5.4. Broader implications

The tectonic evolution of SIA is mainly controlled by two major events: (1) Major and minor plate boundary reorganizations resulting in polarity reversals of the subduction zone, in the SW Pacific and (2) intra-oceanic arc collision with an oceanic plateau. The "Junction Region" has experienced a complex tectonic history (Van de Lagemaat and van Hinsbergen, 2024) with multiple subduction initiation, re-initiations, polarity reversals, and interaction with continental fragments (Buys et al., 2014; Tapster et al., 2014). Isotopic signatures suggest that a mantle boundary separating Indian and Pacific-type mantle domains existed in the SW Pacific as far back as the Late Permian (Nebel et al., 2007). While the Pacific mantle domain is widely accepted as the prevailing upper mantle beneath the eastern margin of the Australian plate at least since the Eocene (Pearce et al., 2007; Todd et al., 2012), the genesis and nature of the Indian mantle domain remain a subject of ongoing debate. Machida et al. (2009) proposed the existence of a geochemical boundary separating the Pacific and Indian type mantle domains. This conceptual boundary was redefined by Qian et al. (2024), who illustrated the Zealandia–Antarctica domain in SE Asia and SW Pacific.

Our revised tectonic reconstruction indicates that arc–plateau collision can trigger a SPR, modify the mantle wedge, and result in mixing of two distinct mantle domains potentially across the broader Junction Region around SIA (Fig. 1). The earlier phase of NE-directed subduction (~62–46 Ma) is reflected by Stage 1 arc magmatism in SIA with Pacific mantle domain affinities on εNd(t) vs εHf(t) co-variation diagram, indicating its dominance up to ~46 Ma beneath SIA. Similar Pacific mantle domain affinities are observed in the early to Island arc tholeiites of the Yavuna Group of Fiji and on "Eua" Tonga, persisting until ~44 Ma (Todd et al., 2012; Marien et al., 2022) and beneath the Malekula segment of the Vanuatu arc till ~20 Ma (Haase et al., 2024b). This implies that the transition from Pacific to Indian-type mantle domain was neither synchronous nor uniform, but instead varied in both spatially and temporally across the region from Solomon Islands to Vanuatu-Fiji-Tonga-Kermadec arcs as a result of continuous tectonic evolution and complex plate reorganization in the SW Pacific since the Cretaceous. This observation suggests that small-scale upper mantle domain boundaries exist. Evidence of rapid mantle wedge replacement driven by mantle corner flow and slab steeping associated with slab rollback has been observed in New Hebrides (Haase et al., 2024a). Likewise, the mantle domain boundary can migrate rapidly at smaller scales. We believe our model provides valuable insights for the complete replacement of one mantle domain by another and trapped mantle domains. Future detailed investigations integrating age, geochemical, and isotopic data will be essential for constraining the spatial evolution of mantle domain boundaries and for elucidating the timescales involved in the replacement of one mantle domain by another.

6. Conclusions

1. Our study identifies three distinct stages of arc magmatism in the SIA, elucidating its spatio-temporal evolution.
2. Stage 1, dated ~46 Ma, is a basic, low-K TH series in Choiseul and Santa Isabel, with N-MORB-like REE pattern and Pacific-like mantle domain affinity associated with the first SPR.
3. Stage 2, at ~35 Ma, is highly silicic, low-K CA granites from Ghizo (NGG), with a flat REE pattern and Indian-like mantle domain affinity reflecting second SPR.
4. Stage 3, spanning medium to high-K CA magmatism between ~19 to 0.7 Ma in the NGG and Choiseul, marks the increasing involvement of OJP-derived material in the Indian-type mantle wedge beneath SIA, indicating the third and latest SPR in SIA.
5. Stages 1–3 indicate derivation from a juvenile mantle source, lacking any crustal contamination, as reflected in zircon Hf isotopes and whole-rock Sr–Nd–Hf data.
6. We constrain the formation age of the NGG basement to ~35 Ma.
7. The initial impingement of the OJP on the NST began around ~20 Ma, triggering a major tectonic reorganization, with the most recent SPR occurring between ~19 and 12 Ma.

Supplementary data to this article can be found online at https://doi.org/10.1016/j.lithos.2025.108281.

CRediT authorship contribution statement

Rashmi Battan: Writing – review & editing, Writing – original draft, Visualization, Investigation, Formal analysis, Data curation. **Sun-Lin Chung:** Writing – review & editing, Writing – original draft, Validation, Supervision, Resources, Investigation, Funding acquisition, Data curation, Conceptualization. **Tsuyoshi Komiya:** Writing – original draft, Investigation, Data curation. **Shigenori Maruyama:** Writing – original draft, Investigation, Conceptualization. **Truong Tai Nguyen:** Data curation. **Hao-Yang Lee:** Writing – original draft, Formal analysis, Data curation. **Yoshiyuki Iizuka:** Validation, Data curation. **Kwan-Nang Pang:** Writing – review & editing, Writing – original draft, Supervision. **Andrew Tien-Shun Lin:** Writing – original draft, Supervision.

Declaration of competing interest

The authors declare that they have no known competing financial interests or personal relationships that could have appeared to influence the work reported in this paper.

The corresponding author SLC declares for all the coauthors that they have no known competing financial interests or personal relationships that could have appeared to influence the work reported in this paper.

Acknowledgments

Battan thanks the Taiwan International Graduate Program (TIGP), Earth System Science and the National Science and Technology Council, Taiwan for the fellowships. This study was supported by the National Science and Technology Council, Taiwan (grant no. 114-2116-M-001-003) and Academic Sinica, Taiwan (grant no. AS-IVA-112-M02) to SLC. We thank K. Okamoto and A. Kadarusman for fieldwork and sample collection, H. Wang for mineral separation, Chien-Hui Hung, Chiu-Hong Chu and You-Jhen Chen for laboratory assistance. We thank the editor and two reviewers for their constructive comments that helped improve the manuscript.

References

Abraham, D.A., Baekisapa, M., Booth, D.J., Dunkley, P.N., Hughes, G.W., Langford, R.L., Philip, P.R., Ridgway, J., Smith, A., Strange, P.J., 1987. New Georgia Group Geological Map Sheet, 1:250 000. Geological Survey Division, Ministry of Natural Resources, Honiara.

Almeida, J., Riel, N., Rosas, F.M., Duarte, J.C., Kaus, B., 2022. Self-replicating subduction zone initiation by polarity reversal. Commun. Earth Environ. 3 (1), 55. https://doi.org/10.1038/s43247-022-00380-2.

Berly, T., 2005. Ultramafic and Mafic Rock Types from Choiseul, Santa Isabel and Santa Jorge (Northeastern Solomon Islands): origins and Significance (Doctoral dissertation). Université Joseph-Fourier-Grenoble I.

Buys, J., Spandler, C., Holm, R.J., Richards, S.W., 2014. Remnants of ancient Australia in Vanuatu: Implications for crustal evolution in island arcs and tectonic development of the Southwest Pacific. Geology 42 (11), 939–942. https://doi.org/10.1130/G36155.1.

Chauvel, C., Blichert-Toft, J., 2001. A hafnium isotope and trace element perspective on melting of the depleted mantle. Earth Planet. Sci. Lett. 190 (3–4), 137–151. https://doi.org/10.1016/S0012-821X(01)00379-X.

Chemenda, A.I., Yang, R.K., Stephan, J.F., Konstantinovskaya, E.A., Ivanov, G.M., 2001. New results from physical modeling of arc–continent collision in Taiwan: evolutionary model. Tectonophysics 333 (1–2), 159–178. https://doi.org/10.1016/S0040-1951(00)00273-0.

Chivas, A.R., McDougall, I., 1978. Geochronology of the Koloula porphyry copper prospect, Guadalcanal, Solomon Islands. Econ. Geol. 73 (5), 678–689. https://doi.org/10.2113/gsecongeo.73.5.678.

Clift, P.D., Schouten, H., Draut, A.E., 2003. A General Model of Arc–continent Collision and Subduction Polarity Reversal from Taiwan and the Irish Caledonides. https://doi.org/10.1144/GSL.SP.2003.219.01.04.

Cloetingh, S., Wortel, R., Vlaar, N.J., 1989. On the initiation of subduction zones. Pure Appl. Geophys. 129 (1), 7–25.

Coleman, P.J., 1962. An outline of the geology of Choiseul, British Solomon Islands. J. Geol. Soc. Aust. 8 (2), 135–157. https://doi.org/10.1080/14400956208527870.

Coleman, P.J., Packham, G.H., 1976. The Solomon Islands and their geology. Bureau of Mineral Resources, Geology and Geophysics. Bulletin 199, 120. Canberra.

Cooper, P.A., Taylor, B., 1985. Polarity reversal in the Solomon Islands arc. Nature 314 (6010), 428–430. https://doi.org/10.1038/314428a0.

Cowley, S., Mann, P., Coffin, M.F., Shipley, T.H., 2004. Oligocene to recent tectonic history of the Central Solomon intra-arc basin as determined from marine seismic reflection data and compilation of onland geology. Tectonophysics 389 (3–4), 267–307.

Crameri, F., Magni, V., Domeier, M., Shephard, G.E., Chotalia, K., Cooper, G., Eakin, C. M., Grima, A.G., Gürer, D., Király, Á., Mulyukova, E., 2020. A transdisciplinary and community-driven database to unravel subduction zone initiation. Nat. Commun. 11 (1), 3750.

Crawford, A.J., Meffre, S., Symonds, P.A., 2003. 120 to 0 ma Tectonic Evolution of the Southwest Pacific and Analogous Geological Evolution of the 600 to 220 ma Tasman Fold Belt System.

Doucet, L.S., Li, Z.X., 2024. Large-scale mantle heterogeneity as a legacy of plate tectonic supercycles. Nat. Geosci. 17 (11), 1175–1181.

Doucet, L.S., Li, Z.X., Gamal El Dien, H., Pourteau, A., Murphy, J.B., Collins, W.J., Mattielli, N., Olierook, H.K., Spencer, C.J., Mitchell, R.N., 2020. Distinct formation history for deep-mantle domains reflected in geochemical differences. Nat. Geosci. 13 (7), 511–515.

Duarte, J.C., Rosas, F.M., Terrinha, P., Schellart, W.P., Boutelier, D., Gutscher, M.A., Ribeiro, A., 2013. Are subduction zones invading the Atlantic? Evidence from the Southwest Iberia margin. Geology 41 (8), 839–842.

Duarte, J.C., Schellart, W.P., Rosas, F.M., 2018. The future of Earth's oceans: consequences of subduction initiation in the Atlantic and implications for supercontinent formation. Geol. Mag. 155 (1), 45–58.

Dunkley, P.N., 1986. Geology of the New Georgia Group, Solomon Islands. Br. Geol. Surv. Overs. Director. 83. Report MP/88/6.

Falvey, D., 1975. Part 2. Younger Pacifics arcs and the eastern marginal seas: Arc reversals, and a tectonic model for the North Fiji Basin. Explor. Geophys. 6 (3), 47–49. https://doi.org/10.1071/EG975047.

Haase, K.M., Regelous, M., Beier, C., Koppers, A.A., 2024a. Slab steepening and rapid mantle wedge replacement during back-arc rifting in the New Hebrides. Nat. Commun. 15 (1), 6070. https://doi.org/10.1038/s41467-024-50445-3.

Haase, K.M., Schneider, K.P., Pelletier, B., Ishizuka, O., 2024b. Magmatic evolution of the fossil Melanesian island arc: Evidence from lower Miocene lavas of Malekula Island (Vanuatu). Geochem. Geophys. Geosyst. 25 (2) e2023GC011187.

Hall, R., 2002. Cenozoic geological and plate tectonic evolution of SE Asia and the SW Pacific: computer-based reconstructions, model and animations. J. Asian Earth Sci. 20 (4), 353–431. https://doi.org/10.1016/S1367 -9120 (01) 00069-4.

Holm, R.J., Spandler, C., Richards, S.W., 2013. Melanesian arc far-field response to collision of the Ontong Java Plateau: geochronology and petrogenesis of the Simuku Igneous complex, New Britain, Papua New Guinea. Tectonophysics 603, 189–212.

Holm, R.J., Rosenbaum, G., Richards, S.W., 2016. Post 8 Ma reconstruction of Papua New Guinea and Solomon Islands: microplate tectonics in a convergent plate boundary setting. Earth Sci. Rev. 156, 66–81. https://doi.org/10.1016/j.earscirev.2016.03.005.

Joshima, M., Okuda, Y., Murakami, F., Kishimoto, K., Honza, E., 1986. Age of the Solomon Sea Basin from magnetic lineations. Geo-Mar. Lett. 6 (4), 229–234.

König, S., Schuth, S., Münker, C., Qopoto, C., 2007. The role of slab melting in the petrogenesis of high-Mg andesites: evidence from Simbo Volcano, Solomon Islands. Contrib. Mineral. Petrol. 153 (1), 85–103. https://doi.org/10.1007/s00410-006-0136-x.

Kroenke, L.W., 1972. Geology of the Ontong Java Plateau. Hawaii Inst. Geophys. Report HIG-72-5, 119.

Kroenke, L.W., 1984. UN ESCAP, CCOP/SOPAC Tech. Bull. Cenozoic Tectonic Development of the Southwest Pacific, p. 6.

Kroenke, L.W., Wessel, P., Sterling, A., 2004. Motion of the Ontong Java Plateau in the Hot-spot Frame of Reference: 122 Ma–Present. https://doi.org/10.1144/GSL.SP.2004.229.01.02.

Le Maitre, R.W., Streckeisen, A., Zanettin, B., Le Bas, M.J., Bonin, B., Bateman, P., 2005. Igneous Rocks: a Classification and Glossary of Terms: recommendations of the International Union of Geological Sciences Subcommission on the Systematics of Igneous Rocks. Cambridge University Press.

Machida, S., Hirano, N., Kimura, J.I., 2009. Evidence for recycled plate material in Pacific upper mantle unrelated to plumes. Geochim. Cosmochim. Acta 73 (10), 3028–3037. https://doi.org/10.1016/j.gca.2009.01.026.

Mann, P., Taira, A., 2004. Global tectonic significance of the Solomon Islands and Ontong Java Plateau convergent zone. Tectonophysics 389 (3–4), 137–190. https://doi.org/10.1016/j.tecto.2003.10.024.

Marien, C.S., Drewes-Todd, E.K., Stork, A., Todd, E., Gill, J.B., Hoffmann, J.E., Tani, K., Allen, C.M., Münker, C., 2022. Juvenile continental crust evolution in a modern oceanic arc setting: Petrogenesis of Cenozoic felsic plutons in Fiji, SW Pacific. Geochim. Cosmochim. Acta 320, 339–365. https://doi.org/10.1016/j.gca.2021.11.033.

Matthews, K.J., Williams, S.E., Whittaker, J.M., Müller, R.D., Seton, M., Clarke, G.L., 2015. Geologic and kinematic constraints on late cretaceous to mid Eocene plate boundaries in the Southwest Pacific. Earth Sci. Rev. 140, 72–107. https://doi.org/10.1016/j.earscirev.2014.10.008.

Mueller, S., Phillips, R.J., 1991. On the initiation of subduction. J. Geophys. Res. Solid Earth 96 (B1), 651–665.

Nebel, O., Münker, C., Nebel-Jacobsen, Y.J., Kleine, T., Mezger, K., Mortimer, N., 2007. Hf–Nd–Pb isotope evidence from Permian arc rocks for the long-term presence of the Indian–Pacific mantle boundary in the SW Pacific. Earth Planet. Sci. Lett. 254 (3–4), 377–392. https://doi.org/10.1016/j.epsl.2006.11.046.

Neef, G., McDougall, I., 1976. Potassium-Argon Ages on Rocks from Small Nggela Island, British Solomon Islands, Southwest Pacific.

Ota, T., Kaneko, Y., 2010. Blueschists, eclogites, and subduction zone tectonics: Insights from a review of late Miocene blueschists and eclogites, and related young high-pressure metamorphic rocks. Gondwana Res. 18 (1), 167–188. https://doi.org/10.1016/j.gr.2010.02.013.

Pearce, J.A., Kempton, P.D., Gill, J.B., 2007. Hf–Nd evidence for the origin and distribution of mantle domains in the SW Pacific. Earth Planet. Sci. Lett. 260 (1–2), 98–114. https://doi.org/10.1016/j.epsl.2007.05.023.

Pearce, J.A., Kempton, P.D., Nowell, G.M., Noble, S.R., 1999. Hf-Nd element and isotope perspective on the nature and provenance of mantle and subduction components in Western Pacific arc-basin systems. J. Petrol. 40 (11), 1579–1611.

Peccerillo, A., Taylor, S.R., 1976. Geochemistry of Eocene calc-alkaline volcanic rocks from the Kastamonu area, northern Turkey. Contrib. Mineral. Petrol. 58 (1), 63–81. https://doi.org/10.1007/BF00384745.

Petterson, M.G., Neal, C.R., Mahoney, J.J., Kroenke, L.W., Saunders, A.D., Babbs, T.L., Duncan, R.A., Tolia, D., McGrail, B., 1997. Structure and deformation of north and Central Malaita, Solomon Islands: tectonic implications for the Ontong Java Plateau-Solomon arc collision, and for the fate of oceanic plateaus. Tectonophysics 283 (1–4), 1–33. https://doi.org/10.1016/S0040-1951(97)00206-0.

Petterson, M.G., Babbs, T., Neal, C.R., Mahoney, J.J., Saunders, A.D., Duncan, R.A., Tolia, D., Magu, R., Qopoto, C., Mahoa, H., Natogga, D., 1999. Geological–tectonic framework of Solomon Islands, SW Pacific: crustal accretion and growth within an intra-oceanic setting. Tectonophysics 301 (1–2), 35–60. https://doi.org/10.1016/S0040-1951(98)00214-5.

Phinney, E.J., Mann, P., Coffin, M.F., Shipley, T.H., 2004. Sequence stratigraphy, structural style, and age of deformation of the Malaita accretionary prism (Solomon arc–Ontong Java Plateau convergent zone). Tectonophysics 389 (3–4), 221–246.

Qian, S., Wu, J.T.J., Wu, J., 2024. Philippine Sea plate and surrounding magmatism reveal the Antarctic-Zealandia, Pacific, and Indian mantle domain boundaries. Commun. Earth Environ. 5 (1), 183. https://doi.org/10.1038/s43247-024-01326-6.

Ramsay, W.R.H., 1972. Geology of the Solomon Islands. N. Z. J. Geol. Geophys. 15 (1), 29–47.

Richards, J.R., Cooper, J.A., Webb, A.W., Coleman, P.J., 1966. Potassium–Argon Measurements of the Age of Basal Schists in the British Solomon Islands. Nature 211 (5055), 1251–1252.

Ridgway, J., 1987. Neogene displacements in the Solomon Islands arc. Tectonophysics 133 (1–2), 81–93. https://doi.org/10.1016/0040-1951(87)90282-4.

Schellart, W.P., Lister, G.S., Toy, V.G., 2006. A late cretaceous and Cenozoic reconstruction of the Southwest Pacific region: tectonics controlled by subduction and slab rollback processes. Earth Sci. Rev. 76 (3–4), 191–233. https://doi.org/10.1016/j.earscirev.2006.01.002.

Schuth, S., Rohrbach, A., Münker, C., Ballhaus, C., Garbe-Schönberg, D., Qopoto, C., 2004. Geochemical constraints on the petrogenesis of arc picrites and basalts, New Georgia Group, Solomon Islands. Contrib. Mineral. Petrol. 148 (3), 288–304.

Schuth, S., Münker, C., König, S., Qopoto, C., Basi, S., Garbe-Schönberg, D., Ballhaus, C., 2009. Petrogenesis of lavas along the Solomon Island Arc, SW Pacific: coupling of compositional variations and subduction zone geometry. J. Petrol. 50 (5), 781–811. https://doi.org/10.1093/petrology/egp019.

Schuth, S., König, S., Münker, C., 2011. Subduction zone dynamics in the SW Pacific plate boundary region constrained from high-precision Pb isotope data. Earth Planet. Sci. Lett. 311 (3–4), 328–338. https://doi.org/10.1016/j.epsl.2011.09.006.

Shinohara, M., Suyehiro, K., Murayama, T., 2003. Microearthquake seismicity in relation to double convergence around the Solomon Islands arc by ocean-bottom seismometer observation. Geophys. J. Int. 153 (3), 691–698. https://doi.org/10.1046/j.1365-246X.2003.01940.x.

Smith, D.J., Petterson, M.G., Saunders, A.D., Millar, I.L., Jenkin, G.R.T., Toba, T., Naden, J., Cook, J.M., 2009. The petrogenesis of sodic island arc magmas at Savo volcano, Solomon Islands. Contrib. Mineral. Petrol. 158 (6), 785–801. https://doi.org/10.1007/s00410-009-0410-9.

Stern, R., 2004. Subduction initiation: Spontaneous and induced. Earth Planet. Sci. Lett. 226, 275–292. https://doi.org/10.1016/j.epsl.2004.08.007.

Stern, R.J., Gerya, T., 2018. Subduction initiation in nature and models: a review. Tectonophysics 746, 173–198.

Stracke, A., Willig, M., Genske, F., Béguelin, P., Todd, E., 2022. Chemical geodynamics insights from a machine learning approach. Geochem. Geophys. Geosyst. 23 (10), e2022GC010606. https://doi.org/10.1029/2022GC010606.

Sun, B., Kaus, B.J., Yang, J., Lu, G., Wang, X., Wang, K., Zhao, L., 2021. Subduction polarity reversal triggered by oceanic plateau accretion: Implications for induced subduction initiation. Geophys. Res. Lett. 48 (24), e2021GL095299.

Sun, S.S., McDonough, W.F., 1989. Chemical and isotopic systematics of oceanic basalts: implications for mantle composition and processes. Geol. Soc. Lond. Spec. Publ. 42 (1), 313–345. https://doi.org/10.1144/GSL.SP.1989.042.01.19.

Tapster, S., Roberts, N.M.W., Petterson, M.G., Saunders, A.D., Naden, J., 2014. From continent to intra-oceanic arc: Zircon xenocrysts record the crustal evolution of the Solomon island arc. Geology 42 (12), 1087–1090. https://doi.org/10.1130/G36033.1.

Tapster, S.R., 2013. A Record of Plateau-Arc Collision: the Crustal and Tectonic Evolution of Guadalcanal, Solomon Islands (Doctoral dissertation). University of Leicester.

Taylor, B., Benyshek, E.K., 2024. Oceanic plateau and spreading ridge subduction accompanying arc reversal in the Solomon Islands. Geochem. Geophys. Geosyst. 25 (1), e2023GC011270. https://doi.org/10.1029/2023GC011270.

Tejada, M.L.G., Mahoney, J.J., Duncan, R.A., Hawkins, M.P., 1996. Age and geochemistry of basement and alkalic rocks of Malaita and Santa Isabel, Solomon Islands, southern margin of Ontong Java Plateau. J. Petrol. 37 (2), 361–394. https://doi.org/10.1093/petrology/37.2.361.

Tejada, M.L.G., Mahoney, J.J., Neal, C.R., Duncan, R.A., Petterson, M.G., 2002. Basement geochemistry and geochronology of Central Malaita, Solomon Islands, with implications for the origin and evolution of the Ontong Java Plateau. J. Petrol. 43 (3), 449–484. https://doi.org/10.1093/petrology/43.3.449.

Teng, L.S., Lee, C.T., Tsai, Y.B., Hsiao, L.Y., 2000. Slab breakoff as a mechanism for flipping of subduction polarity in Taiwan. Geology 28 (2), 155–158. https://doi.org/10.1130/0091-7613(2000)28%3C155:SBAAMF%3E2.0.CO;2.

Todd, E., Gill, J.B., Pearce, J.A., 2012. A variably enriched mantle wedge and contrasting melt types during arc stages following subduction initiation in Fiji and Tonga, Southwest Pacific. Earth Planet. Sci. Lett. 335, 180–194. https://doi.org/10.1016/j.epsl.2012.05.006.

Van de Lagemaat, S.H., van Hinsbergen, D.J., 2024. Plate tectonic cross-roads: reconstructing the Panthalassa-Neotethys Junction Region from Philippine Sea Plate and Australasian oceans and orogens. Gondwana Res. 126, 129–201. https://doi.org/10.1016/j.gr.2023.09.013.

Whattam, S.A., Malpas, J., Ali, J.R., Smith, I.E., 2008. New SW Pacific tectonic model: Cyclical intraoceanic magmatic arc construction and near-coeval emplacement along the Australia-Pacific margin in the Cenozoic. Geochem. Geophys. Geosyst. 9 (3).

Yang, G., 2022. Subduction initiation triggered by collision: a review based on examples and models. Earth Sci. Rev. 232, 104129. https://doi.org/10.1016/j.earscirev.2022.104129.